Photonic titanium dioxide film obtained from hard template with chiral nematic structure for environmental application

Chunyu Li, Erwan Paineau, Francois Brisset, Sylvain Franger, Christophe Colbeau-Justin, Mohamed Nawfal Ghazzal

Photonic Titanium dioxide film obtained from hard template with chiral nematic structure for environmental application

Chunyu Li,[a] Erwan Paineau,[b] François Brisset,[c] Christophe Colbeau-Justin,[a] Mohamed N. Ghazzal [a] *

[a] Laboratoire de Chimie Physique, UMR 8000 CNRS, Université Paris-Sud, Université Paris-Saclay 91405 Orsay, France
[b] Laboratoire de Physique du Solide, UMR 8502 CNRS, Université Paris-Sud, Université Paris-Saclay 91405 Orsay, France
[c] Institut de ChimieMoléculaireetdesMatériauxd'Orsay(ICMMO),Université de Paris-Sud, Université Paris-Saclay, Orsay 91405, France

E-mail: mohamed-nawfal.ghazzal@u-psud.fr

Abstract

In the present work, mesoporous TiO_2 with a photonic structure was elaborated using cellulose nanocrystals (CNCs) as a biotemplate by two-step hard template methods. This strategy enables to replicate the chiral nematic (CN) structure of the photonic films (biotemplate) in TiO_2 films. A series of iridescent CNCs films with different weight ratios of silica/CNCs composite photonic films were prepared via evaporation induced self-assembly (EISA) method. The films showed iridescent color and tuneable Bragg reflection wavelengths by solely changing the ratio between the silica and the CNCs biotemplate. Polarized optical microscopy (POM) performed on hydride SiO_2/CNCs films showed a birefringence and typical fingerprint of chiral nematic structure. This birefringence was also observed for TiO_2 films obtained using SiO_2 films as a hard template, which suggested the transfer of the chiral nematic structure in TiO_2 materials. Afterwards, their optical, morphological and electronic properties were studied by scanning electron microscope (SEM), POM, energy-dispersive X-ray spectroscope (EDX) and time resolved microwave conductivity (TRMC). The photocatalytic activities were evaluated by following the phenol degradation using high performance liquid chromatography (HPLC). The results showed that the structuration of the TiO_2 film using a chiral nematic SiO_2 film as hard template enhances the photocatalytic performance compared to non-structured mesoporous TiO_2.

Key words: cellulose nanocrystals, light harvesting, evaporation induced self-assembly, iridescent film, chiral nematic structure, hard template, phenol degradation.

Introduction

Photocatalysis is attracting more and more attention owing to its environmentally friendly approach toward the conversion of light energy into chemical energy and under mild reaction environments. Photocatalysis is considered as a promising solution to energy shortage or environmental issues and has been successfully applied in a wide range of applications, ranging from hydrogen production [1–3] to pollutants elimination [4–6] or for CO_2 reduction [7,8]. Among all the semiconductors (SC) used for photocatalysis, TiO_2 remains the most widely used SC, recognized for, low cost, high chemical stability throughout a wide pH range and robustness under UV illumination. However, because of its wide band-gap (3.2 eV for anatase), it can only absorb in the UV light (< 400 nm), which accounts for 3-5% of the total solar energy reaching the earth's surface, but also involves a fast recombination of electron-hole pairs [9,10]. Thus, the practical application of pure TiO_2 as photocatalyst (PC) materials is seriously impeded. To tackle this issues, various strategies have been adopted in the last decade, for improving the photocatalytic efficiency of TiO_2 in particular by coupling with other seminconductors [11,12] and metallic co-catalyst nanoparticles [2,13–16]. Furthermore, considering the speed of light ($\sim 1-3 \times 10^8$ m s^{-1}) passing through nanosized TiO_2 photocatalyst, it leaves less than hundred femtoseconds to TiO_2 to be activated.

One strategy that appears very efficient is to design TiO_2 in a photonic structure, which requires neither the modification of TiO_2 nor the coupling with other semiconductors. The pioneering work of Yablonovich proposed the basics of the extraordinary properties of photonic crystals (PCs) [17]. The optical enhancement properties of photonic crystals focused on solar-energy applications have been extensively explored these years [18–23]. Depending on geometry of the structure, photonic crystals can be divided into one-dimensional (1D), two-dimensional (2D) and three-dimensional (3D) structures. In particular, 3D artificial photonic crystals are considered as one of the most potential materials due to their permittivity modulation along all three directions. Furthermore, their complete photonic band-gap could reflect electromagnetic waves in all directions [24,25]. It is well-recognized that photonic nanostructures improve the Bragg scattering in the material and have the ability to reduce the group velocity of photons [26]. This interesting concept applied to photocatalytic system was suggested some years ago by combining, in the same structure, the optical properties of photonic crystals with the unique

photocatalytic behaviour of TiO_2 [27–34]. This appealing idea could be used to design photocatalytic systems of SC materials with enhanced light interaction time, resulting in higher photogenerated charge carriers through “slow-photon effect”. In this case, the energy of the slow photons must overlap with the absorbance spectrum of the semiconductor [29,33]. Interestingly, slowing down the photon motion also increase the optical path length. Hence, TiO_2 would have more time to absorb photons leading to higher photogenerated electron-hole pairs density (enhancement of the absorbance factor).

Up to now, opal, inverse opal and butterfly wings have been extensively used as an organic template to fabricate photonic materials [27,35,36]. Many researches reported the synthesize of photonic TiO_2 with opal or inverse opal fashion. Synthesis of 3D inverse opal TiO_2 photonic crystals with large surface area using polystyrene opal templates in sandwich method or using convective self-assembly of polystyrene microspheres by repeat atomic layer deposition of titanium dioxide were reported [37,38]. TiO_2-based photocatalysts fashioned as inverse opals with tuneable Bragg peak reflection showed an enhancement of the photocatalytic activity for dyes degradation [29,36]. The photoactivity improvement was attributed to the intensified dye sensitization because of slow photon effect on the red and blue edges of the photonic band-gaps [30]. The photocatalytic activity of PC materials formed from phototonic crystals showed a dependence of the illumination wavelength and the irradiation angle. Thus, the irradiation wavelength matching the blue or the red edges of the Bragg reflection showed highest photoactivity for dye degradation. Meanwhile, synthesis of biomorphic TiO_2 photonic crystals were explored by using butterfly wings as a template and the subsequent deposition of gold nanoparticles as co-photocatalyst, that show a significant increase for the photodecomposition of methyl orange dye under visible light illumination [27]. Coupling slow photon effect with surface plasmon resonance enhances the photocatalytic activity.

In this study, titanium dioxide as a photocatalyts was elaborated using mesoporous silica film with chiral nematic structure as a hard template. The Bragg reflection of the hard template was tuned using variable ratio of SiO_2/CNCs in the visible light. The obtained TiO_2 showed a birefringence suggesting a transfer of the 3D structure from the hard template to the photocatalyst. The study of the dynamic of photogenerated charges and the photocatalytic properties showed an enhancement of the light harvesting and the photoefficiency.

Experimental section

Materials

All chemicals were used as received without further purification. Titanium isopropoxide (TTIP, 97%), Tetraethyl orthosilicate (TEOS, 98%), and cellulose nanocrystals were extracted from pure ramie fibers as previously reported [39] and ethanol was purchased from VWR Chemicals. Deionized water (Milli-Q water under 18.2 MΩ) was used in the experiment.

Synthesis of SiO_2/CNCs composite films with chiral nematic structure

The composite films were prepared following the procedure reported elsewhere [40,41]. Briefly, the composite films were obtained by combining the CNCs (3.3 wt%) and TEOS *via* evaporation induced self-assembly method (EISA). TEOS were mixed with 1 ml ethanol under stirring at room temperature for 10 min and then added dropwise to 5 mL of aqueous CNCs solution, readily sonicated for 10 min. The TEOS/CNCs weight ratios were ranged from 0.5 to 3 wt% as detailed in Table 1. The solution was aged under stirring for 1 hour at room temperature before free-casting the solution in petri dishes.

Table 1. Compositions of silica/CNCs films with different weight ratio

Sample	Weight ratio SiO_2/CNCs	TEOS (ml)	Ethanol (mL)	Calculated SiO_2 (g)	3.3 wt% 5mL CNCs (g)
SiO_2/CNC-0.5	0.5	0.3	1	0.08	0.17
SiO_2/CNC-1	1	0.58	1	0.17	0.17
SiO_2/CNC-2	2	1.16	1	0.33	0.17
SiO_2/CNC-3	3	1.74	1	0.45	0.17

Two-step hard template method

The protocol used in this work was inspired by the method detailed in [42]. Mesoporous silica films with chiral nematic structure were elaborated by the calcination of silica/CNCs nanocomposite films. The nanocomposite films were dried at 150 °C for 2 h and then at 500 °C during 4 h with a rate of 2 °C.min^{-1}. An aqueous TTIP-HCl solution was loaded into the mesoporous silica films using the incipient wetness method. After each loading step, the films

were dried and annealed at 180°C. After five impregnation/drying cycles, the silica/titania films were calcined at 500°C for 4h to obtain a crystalline product. The silica templates were then removed by dissolving them in 2M $NaOH_{(aq)}$ for 1 day, resulting in mesoporous TiO_2 film with photonic structure.

Characterization

The morphologies and nanostructures of synthesized samples were characterized by scanning electron microscope (SEM) ZEISS Supra 55VP FEG-SEM at 1 kV scanning electron microscope operating at 2 kV and working distance between 3 and 5.7 mm.

The purity of CNC was controlled by Wide-Angle X-Ray Scattering (WAXS) experiments. Measurement was carried out on a copper rotating anode generator ($\lambda_{Cu\ K\alpha}$ = 1.5418 Å, Rigaku Corp., Japan) monochromatized with a multilayer W/Si optics (Osmic) a monochromatic beam of 1 x 1 mm² at the sample position [43]. Two-dimensional WAXS pattern was collected on a MAR345 detector (marXperts GmbH, Germany) with 150 µm pixel size, placed at a sample-to-detector distance of 200 mm. The typical accessible range of scattering vector modulus Q was 0.1 – 3 $Å^{-1}$ ($Q = 4\pi/\lambda \sin(\theta)$, where λ is the incident wavelength and 2θ is the scattering angle). Scattered intensity I as a function of the scattering vector modulus Q is obtained by angular integration over the 2D scattering patterns using homemade software. Experimental resolution can be approximated by a Gaussian with Full-Width at Half Maximum (FWHM) ~0.013 $Å^{-1}$.

Optical properties of CNC-based films were studied using UV-Vis-NIR spectroscopy (model Cary 5000 series from Agilent Technologies) equipped with an integrating sphere for diffuse and total reflection measurements. The diffuse-reflectance spectra were recorded by mounting the film perpendicular to the beam light. The maximum reflectance was set to 100% using $BaSO_4$ as a reference in a wavelength ranged between 300 to 800 nm.

Polarized optical microscopy (POM) observations were obtained at room temperature using a ZEISS Axio Observer Z1 equipped with 10× (0.25 NA), 20× (0.5 NA) and 40× (0.6 Korr) objectives. The images were recorded using ZEN software 3.2 lite.

The dynamics of charge-carrier and lifetimes in TiO_2 were determined by microwave absorption experiments using the Time Resolved Microwave Conductivity (TRMC) method after UV illumination (λ_{max}=360 nm) [44]. After the illumination by means a laser pulse, free

photogenerated electrons and holes leads to a perturbation of the initial microwave absorbance. The temporal evolution of conductivity signal reflected by the sample is related to the lifetime of the photogenerated carriers, which can be evaluated considering the following equation:

$$\frac{\Delta P(t)}{P} = A\Delta\sigma(t) = Ae\sum\Delta n_i(t)\mu_i \qquad (1)$$

where $\Delta n_i(t)$ is the number of excess charge-carriers i at time t and μ_i is their mobility. The sensitivity factor A.

The photocatalytic activity of synthesized TiO_2 was evaluated by following the photodegradation of phenol as a probe molecule in water (50 ppm) under UV-vis illumination using a Xenon lamp (Oriel 300 W). The photocatalytic degradation of phenol was carried out in a quartz reactor ($1 \times 1 \times 4.5$ cm^3) using 3.5 mg of photocatalyst suspended in 3.5 mL of an aqueous solution. During the photocatalytic experiments, the solution was continuously stirred and bubbled a fixed flow of oxygen. Before starting the photocatalytic test, the slurry solution was aged for 20 minutes under magnetic stirring in the dark to reach the adsorption and desorption equilibrium. The phenol concentration was followed by HPLC (Agilent 1260 infinity quaternary liquid chromatograph) equipped with a UV detector set at 260 nm for phenol analysis.

Results and discussions

Cellulose nanocrystal

Cellulose nanocrystal extracted from tunicate under sulfuric acid hydrolysis were used to synthesize the photonic films with evaporation induced self-assembly method. During acid hydrolysis, the sulfate ester group (CNC-OSO_4H) replaces the hydroxyl group (CNC-OH) of cellulose [45]. The morphology of the CNCs after extraction has been determined by SEM observations (Figure 1a). The image shows agglomerated rod-like nanocrystals, which the diameter of each nanorode is estimated to be ranged in 200-300 nm in length. The crystallinity of CNC sample was assessed by WAXS measurements. WAXS diagram presents a sharp peak at Q = 1.604 Å^{-1} (d-spacing d = 3.92 Å) and two overlapping peaks at Q = 1.051 Å^{-1} (d = 5.98 Å) and Q = 1.175 Å^{-1} (d = 5.35 Å), corresponding to the (100), $(1\bar{1}0)$ and (110) planes, respectively, characteristics of cellulose I_β without any other by-products [46].

Preparation of Mesoporous Silica as a hard template

Hybrid solution containing silica precursor and CNCs was prepared in water. The negatively charged sulfate group creates an electrostatic repulsion form isotropic and anisotropic phase []. A well-ordered hybrid mesostructured SiO_2/CNCs is obtained after free casting the solution by using the EISA method. It is well-known that CNC form spontaneously birefringent chiral nematic droplets (or tactoids) when dispersed in suspensions [47]. In the present case, upon evaporation of the solvent, the tactoids coalesce leading to the self-organization of CNCs together with a polycondensation of the TEOS precursor [40,48]. The self-assembly process was performed at pH = 4.8, which was found to be a critical parameter for the stabilization of the chiral nematic structure. Indeed, the pH of the solution in composite films is preferred to be near the isoelectric point of silica material . SiO_2/CNCs composite films are fisrt characterizad by polarized optical microscopy (Figures 2a-d). Whatever the SiO_2/CNCs weight ratio, all composite films display strong birefringence. However, the birefringence is not homogeneous but rather presents a patchwork of regions of different blue-purple color with macrodomaines differing by their size, which is typical of spherulitic behavior of fibrillar crystals in which the molecules are packed with their axes perpendicular to the fibrillar axis [49]. Furthermore, the fingerprint of chiral nematic structutre are clearly visible (Figure 2.b) confirming the formation of the 3D structure during the EISA. To clearly determine the organization of CNCs in the resulting film, cross section of a hybrid SiO_2/CNCs film (SiO_2/CNCs-2) was observed by SEM (Figure 2.e). Successive bands are observed, which correspond to the twist of periodic CNCs structure, perpendicular to the surface of the films, similar to that observed in pure chiral nematic CNC film [50]. This observation confirms the presence of a chiral nematic ordering in the SiO_2/CNCs composite films.

EISA method enables to elaborate iridescent film with good homogeneity as showed in Figure 3a-d. Based on the Bragg law, when the half of helical pitch much exactly equal to the wavelength of incident light, the light cannot propagate through the material but it is rather reflected. Thus, the films display iridescent color due to the light reflecting in the visible region. Figure 4a presents the UV-visible spectra recorded for the hybrid films prepared at different wieght ratio. The maximum wavelength of the Bragg peak reflection is red-shifted with increasing silica/CNCs weight ratio. The two components of the composite silica/CNCs films, SiO_2 and crystalline cellulose, have similar refractive index (n = 1.46 and 1.54, respectively). One can therefore expect only small variation of the *average* refarctive index, when CNCs and SiO_2 are associated in the resulting composite films. In the present case, the observed red-shift must be predominantly caused by the increase in helica pitch *P* between CNCs with increasing

the silica content. Indeed, SiO_2 coveres the CNCs nanoparticles and thus increases the helical pitch [41]. After calcination at 500°C, the cellulose nanocrystals are mineralized and the resulting silica films with a chiral nematic structure are obtained. Indeed, POM observations depicted in Figure 4a clearly highligth the irridescence caused by the the retention of the chiral nematic structure in the inorganic SiO_2 films. Furthermore, higher magnification of Figure 4b evidences the fingerprint texture caracteristic of the chiral nematic ordering.

Nanocrystalline TiO_2 obtained from hard templating of SiO_2 with chiral nematic structure

Hard template method has been used to elaborate mesoporous TiO_2 with chiral nematic structure. The cellulose biotemplate was removed by both calcination of silica/CNCs films at 500 °C under air. After filling the porous SiO_2 structure with titanium precursor, the silica was selectively etched under highly basic solution leaving only inorganic mesoporous TiO_2 films. EDX analysis of the HT-TiO_2 is presented in Figure 5.a showing that the etching process removed efficiently the silica hard template. Indeed, only TiO_2 was observed and no silica was present in the material with a trace of Na and Cl left due to the acidic medium used for the TTIP stabilization and the after the basic treatment used for the silica etching. The morphology of the cross section of the films has been analyzed by SEM (Figure 5.b). The film presents a mesoporous structure with a size about of 5-15 nm in correlation with the expected diameter of the initial CNCs biotemplate. However, these observations the hierarchical mesostructured of the film shows no evidence of the helicoidal chiral nematic structure. This would be attributed to the orientation of the films during the SEM analysis.

POM micrographs were used to study the synthesized TiO_2 after etching SiO_2 under basic solution. Polarized light is a contrast-enhancing technique that improves the quality of the image obtained with birefringent materials that can be useful for both quantitative and qualitative studies for a wide range of anisotropic specimens. POM observation of HT-TiO_2 using POM, the films show typical birefringence of TiO_2 with chiral nematic structure as reported elsewhere [42]. The strongly birefringent of the films suggested the long-range anisotropy of TiO_2 with the retention of the hierarchical structure. The color evolving from silver (Figure 6.a and 6.b), gold (Figure 6.c) to clear blue (Figure 6.d). The color change could be due to selective reflection, since the variable initial Bragg peak position of the composite SiO_2/CNCs used as a hard template were used (showed in Figure 3).

Photophysical and photocatalytic properties of synthesized TiO_2 nanomaterials

Time Resolved Microwave Conductivity (TRMC)

Electronic property of the synthesized TiO_2 was studied by TRMC technique. TRMC is used to study the excess of photogenerated charge-carriers and their dynamics [44,51]. The charge-carrier dynamics (electronic properties) of the samples were studied at the excitation wavelength at 360 nm. The laser energies reaching the samples was 1.3 $mJ.cm^{-2}$. The TRMC signal is mainly due to mobile electrons reaching the surface after excitation. After the illumination of TiO_2, electron and hole are produced, which modify the conductivity of the semiconductor. Knowing that holes are heavier than electrons with limited mobility, they remain localized in the bulk. Thus, the TRMC signal is mainly due to electrons [52]. The signal display the apparition of charge-carriers during the pulse and their lifetime (decay) after the pulse by phenomena; such as recombination or trapping. TRMC signals of HT-TiO_2 samples obtained from variable hard template showing Bragg peaks reflection with variable wavelength maximum is displayed Figure 7.a. The TRMC signal shows an increase of the intensity right after the illumination indicating a large photogenerated charge carriers. After 20 s, the signal decay suggested a recombination and surface trapping of the photogenerated charges. As a comparison, and in order to highlight the effect of the transferred helicoidal chiral structure into the TiO_2 film on the photogenerated charges, mesoporous TiO_2 film with no chiral nematic structure was prepared by one-pot method (mesoTiO_2). The intensity of the TRMC signals of the HT-TiO_2 under UV illumination 4 fold-higher compared to the mesoporous TiO_2 films synthesized by one-pot method. These results highlight the beneficial effect of the chiral nematic structure on the charge-carriers density produced after each excitation. Higher TRMC signal intensity indicates that the density of electrons produced at the surface is enhanced. The 3D structure act as an optical cavity, which increases the light scattering in the photonic film. These results indicate that the modified TiO_2 harvest more light by taking advantage of slow photon effect or scattering effect. Furthermore, compared with mesoporous TiO_2 films, the decay of ImTiO_2 show faster decay, which can be attributed to high trapping sites ratio in the mesostructure.

Photocatalytic degradation of Phenol

The photoactivities of the photonic TiO_2 through two-step hard template were evaluated by following the degradation of phenol under UV-visible illumination. Before illumination, no adsorption was observed after stirring the solution in dark. The films elaborated using the hard template method "HT-TiO_2" showed better photocatalytic efficiency compared to mesoTiO_2 film, except the one obtained with ratio 0.5. Optimal photocatalytic efficiency was observed for

HT-TiO_2 obtained using the weight ratio 2 and up to 70 % of the phenol was decomposed after 2 h. The photoefficiency is 1.5 fold-higher for that sample (HT-TiO_2-2), a sample that also shows higher production of charge carriers density. The enhancement of the photocatalytic activity could be correlated to the enhancement of the improvement of the photogenerated charge carriers evidenced by TRMC. The improvement of the light scattering combined to the slow-photon effect increase the time that illumination photons are in contact with TiO_2. This enables TiO_2 to increase its light harvesting leading to higher production of photogenerated charge carriers. In solution, the production of higher concentration of OH° and $O_2^{\circ-}$ responsible to the degradation of phenol enhance the kinetic of photocatalytic reaction. Thus, the improvement of the photocatalytic efficiency is due to the improvement of the light harvesting due multiple scattering or "slow-photon effect".

Conclusion

In the present work, different methods were successfully used to elaborate TiO_2 film showing a birefringence indicating the retention of helicoidal structure using hard template method. The resultant photocatalysts were elaborated using hard silica film, already obtained using variable ratio and showing tuneable stopbands. The photonic TiO_2 films were synthesized with a primary aim to improving light harvesting process in photocatalysis. The replicas of chiral nematic structure were confirmed by POM and SEM. We also investigate electronic properties of our samples by TRMC. It was found that by taking advantage of the photonic film, HT-TiO_2 films exhibited higher light-harvesting efficiency than the mesoTiO_2. This enhancement can be attributed to the increase of light scattering or slow photon effect, which is was found in agreement with the photocatalytic efficiency improvement.

Acknowledgements
MNG is grateful to Marie-Claire Schanne-Klein from "Laboratoire d'optique et biosciences", université Paris-Saclay, for the full access to the polarized optical microscope and to Youssef Habibi from "Department of Materials Research and Technology (MRT)", Luxembourg, for cellulose nanocrystals samples.

References

[1] J.-J. Chen, J.C.S. Wu, P.C. Wu, D.P. Tsai, Plasmonic Photocatalyst for H 2 Evolution in Photocatalytic Water Splitting, J. Phys. Chem. C. 115 (2011) 210–216. doi:10.1021/jp1074048.

[2] S. Linic, P. Christopher, D.B. Ingram, TiN Modulator 45 Plasmonic-metal

nanostructures for efficient conversion of solar to chemical energy, Nat. Mater. 10 (2011) 911–921. doi:10.1038/nmat3151.

[3] S. Wang, Y. Gao, S. Miao, T. Liu, L. Mu, R. Li, F. Fan, C. Li, Positioning the Water Oxidation Reaction Sites in Plasmonic Photocatalysts, J. Am. Chem. Soc. 139 (2017) 11771–11778. doi:10.1021/jacs.7b04470.

[4] M.N. Ghazzal, H. Kebaili, M. Joseph, D.P. Debecker, P. Eloy, J. De Coninck, E.M. Gaigneaux, Photocatalytic degradation of Rhodamine 6G on mesoporous titania films: Combined effect of texture and dye aggregation forms, Appl. Catal. B Environ. 115–116 (2012) 276–284. doi:10.1016/j.apcatb.2011.12.016.

[5] N.M. Ghazzal, N. Chaoui, E. Aubry, a. Koch, D. Robert, A simple procedure to quantitatively assess the photoactivity of titanium dioxide films, J. Photochem. Photobiol. A Chem. 215 (2010) 11–16. doi:10.1016/j.jphotochem.2010.07.014.

[6] C. Guillard, D. Baldassare, C. Duchamp, M.N. Ghazzal, S. Daniele, Photocatalytic degradation and mineralization of a malodorous compound (dimethyldisulfide) using a continuous flow reactor, Catal. Today. 122 (2007) 160–167. doi:10.1016/j.cattod.2007.01.059.

[7] K. Li, X. An, K.H. Park, M. Khraisheh, J. Tang, A critical review of CO2photoconversion: Catalysts and reactors, Catal. Today. 224 (2014) 3–12. doi:10.1016/j.cattod.2013.12.006.

[8] K. Li, B. Peng, T. Peng, Recent Advances in Heterogeneous Photocatalytic CO_2 Conversion to Solar Fuels, ACS Catal. 6 (2016) 7485–7527. doi:10.1021/acscatal.6b02089.

[9] Y. Tamaki, A. Furube, M. Murai, K. Hara, R. Katoh, M. Tachiya, Dynamics of efficient electron–hole separation in TiO_2 nanoparticles revealed by femtosecond transient absorption spectroscopy under the weak-excitation condition, Phys. Chem. Chem. Phys. 9 (2007) 1453–1460. doi:10.1039/B617552J.

[10] M.N. Ghazzal, E. Aubry, N. Chaoui, D. Robert, Effect of SiN_x diffusion barrier thickness on the structural properties and photocatalytic activity of TiO_2 films obtained by sol-gel dip coating and reactive magnetron sputtering, Beilstein J. Nanotechnol. 6 (2015). doi:10.3762/bjnano.6.207.

[11] Y. Bessekhouad, N. Chaoui, M. Trzpit, N. Ghazzal, D. Robert, J.V. Weber, UV–vis versus visible degradation of Acid Orange II in a coupled CdS/TiO_2 semiconductors suspension, J. Photochem. Photobiol. A Chem. 183 (2006) 218–224. doi:10.1016/j.jphotochem.2006.03.025.

[12] M.N. Ghazzal, R. Wojcieszak, G. Raj, E.M. Gaigneaux, Study of mesoporous CdS-quantum-dot-sensitized TiO_2 films by using X-ray photoelectron spectroscopy and AFM, Beilstein J. Nanotechnol. 5 (2014) 68–76. doi:10.3762/bjnano.5.6.

[13] M. Liu, X. Qiu, M. Miyauchi, K. Hashimoto, Energy-level matching of Fe(III) ions grafted at surface and doped in bulk for efficient visible-light photocatalysts, J. Am. Chem. Soc. 135 (2013) 10064–10072. doi:10.1021/ja401541k.

[14] M. Liu, R. Inde, M. Nishikawa, X. Qiu, D. Atarashi, E. Sakai, Y. Nosaka, K. Hashimoto, M. Miyauchi, Enhanced photoactivity with nanocluster-grafted titanium dioxide photocatalysts, ACS Nano. 8 (2014) 7229–7238. doi:10.1021/nn502247x.

[15] E. Kowalska, R. Abe, B. Ohtani, Visible light-induced photocatalytic reaction of gold-modified titanium(iv) oxide particles: action spectrum analysis, Chem. Commun. (2009) 241–243. doi:10.1039/B815679D.

[16] S.W. Verbruggen, M. Keulemans, M. Filippousi, D. Flahaut, G. Van Tendeloo, S. Lacombe, J.A. Martens, S. Lenaerts, Plasmonic gold-silver alloy on TiO2photocatalysts with tunable visible light activity, Appl. Catal. B Environ. 156–157 (2014) 116–121. doi:10.1016/j.apcatb.2014.03.027.

[17] E. Yablonovitch, Inhibited Spontaneous Emission in Solid State Physics and Electronics, Phys. Rev. Lett. 58 (1987) 2059. doi:10.1103/PhysRevLett.18.395.

[18] A. Mihi, H. Miguez, Origin of light-harvesting enhancement in colloidal-photonic-crystal-based dye-sensitized solar cells, J. Phys. Chem. B. 109 (2005) 15968–15976. doi:10.1021/jp051828g.

[19] S. Guldin, S. Hüttner, M. Kolle, M.E. Welland, P. Müller-Buschbaum, R.H. Friend, U. Steiner, N. Tétreault, Dye-sensitized solar cell based on a three-dimensional photonic crystal, Nano Lett. 10 (2010) 2303–2309. doi:10.1021/nl904017t.

[20] A. Mihi, C. Zhang, P. V. Braun, Transfer of preformed three-dimensional photonic crystals onto dye-sensitized solar cells, Angew. Chemie - Int. Ed. 50 (2011) 5712–5715.

doi:10.1002/anie.201100446.

[21] S. Nishimura, N. Abrams, B.A. Lewis, L.I. Halaoui, T.E. Mallouk, K.D. Benkstein, J. Van de Lagemaat, A.J. Frank, Standing wave enhancement of red absorbance and photocurrent in dye-sensitized titanium dioxide photoelectrodes coupled to photonic crystals, J. Am. Chem. Soc. 125 (2003) 6306–6310. doi:10.1021/ja034650p.

[22] L.I. Halaoui, N.M. Abrams, T.E. Mallouk, Increasing the Conversion Efficiency of Dye-sensitized TiO2 Photoelectrochemical Cells by Coupling to Photonic Crystals., J. Phys. Chem. B. 109 (2005) 6334–42. doi:10.1021/jp044228a.

[23] K. Xie, M. Guo, H. Huang, Photonic crystals for sensitized solar cells: fabrication, properties, and applications, J. Mater. Chem. C. 3 (2015) 10665–10686. doi:10.1039/C5TC02121A.

[24] M.N. Ghazzal, O. Deparis, a. Errachid, H. Kebaili, P. Simonis, P. Eloy, J.P. Vigneron, J. De Coninck, E.M. Gaigneaux, Porosity control and surface sensitivity of titania/silica mesoporous multilayer coatings: applications to optical Bragg resonance tuning and molecular sensing, J. Mater. Chem. 22 (2012) 25302. doi:10.1039/c2jm35107b.

[25] M.N. Ghazzal, M. Joseph, H. Kebaili, J. De Coninck, E.M.M. Gaigneaux, Tuning the selectivity and sensitivity of mesoporous dielectric multilayers by modifiying the hydrophobic–hydrophilic balance of the silica layer, J. Mater. Chem. 22 (2012) 22526. doi:10.1039/c2jm33692h.

[26] J.I.L. Chen, E. Loso, N. Ebrahim, G.A. Ozin, Supporting information for Synergy of Slow Photon and Chemically Amplified Photochemistry in Platinum Nanocluster Loaded Inverse Titania Opals Jennifer I. L. Chen, Edward Loso, Naazia Ebrahim and Geoffrey A. Ozin, (n.d.) 1–9.

[27] Y. Wang, D.B. Xiong, W. Zhang, H. Su, Q. Liu, J. Gu, S. Zhu, D. Zhang, Surface plasmon resonance of gold nanocrystals coupled with slow-photon-effect of biomorphic TiO2photonic crystals for enhanced photocatalysis under visible-light, Catal. Today. 274 (2016) 15–21. doi:10.1016/j.cattod.2016.01.052.

[28] J. Liu, H. Zhao, M. Wu, B. Van der Schueren, Y. Li, O. Deparis, J. Ye, G.A. Ozin, T. Hasan, B.L. Su, Slow Photons for Photocatalysis and Photovoltaics, Adv. Mater. 29 (2017) 1–21. doi:10.1002/adma.201605349.

[29] M. Wu, J. Jin, J. Liu, Z. Deng, Y. Li, O. Deparis, B.-L. Su, High photocatalytic activity enhancement of titania inverse opal films by slow photon effect induced strong light absorption, J. Mater. Chem. A. 1 (2013) 15491. doi:10.1039/c3ta13574h.

[30] O. Deparis, S.R. Mouchet, B.-L. Su, Light harvesting in photonic crystals revisited: why do slow photons at the blue edge enhance absorption?, Phys. Chem. Chem. Phys. 17 (2015) 30525–30532. doi:10.1039/C5CP04983K.

[31] X. Zhang, Y. Liu, S.-T. Lee, S. Yang, Z. Kang, Coupling surface plasmon resonance of gold nanoparticles with slow-photon-effect of TiO2 photonic crystals for synergistically enhanced photoelectrochemical water splitting, Energy Environ. Sci. 7 (2014) 1409. doi:10.1039/c3ee43278e.

[32] J.I.L. Chen, G.A. Ozin, Tracing the effect of slow photons in photoisomerization of azobenzene, Adv. Mater. 20 (2008) 4784–4788. doi:10.1002/adma.200801833.

[33] J.I.L. Chen, G. Von Freymann, S.Y. Choi, V. Kitaev, G.A. Ozin, Amplified photochemistry with slow photons, Adv. Mater. 18 (2006) 1915–1919. doi:10.1002/adma.200600588.

[34] H. Zhao, Z. Hu, J. Liu, Y. Li, M. Wu, G. Van Tendeloo, B.L. Su, Blue-edge slow photons promoting visible-light hydrogen production on gradient ternary 3DOM TiO2-Au-CdS photonic crystals, Nano Energy. 47 (2018) 266–274. doi:10.1016/j.nanoen.2018.02.052.

[35] F. Sordello, V. Maurino, C. Minero, Improved Photochemistry of TiO_2 Inverse Opals and some Examples, Mol. Photochem. – Var. Asp. (2007) 63–86. doi:10.5772/38768.

[36] J.I.L.L. Chen, E. Loso, N. Ebrahim, G.A. Ozin, Synergy of slow photon and chemically amplified photochemistry in platinum nanocluster-loaded inverse titania opals, J. Am. Chem. Soc. 130 (2008) 5420–5421. doi:10.1021/ja800288f.

[37] Z. Gu, A. Fujishima, O. Sato, Fabrication of High-Quality Opal Films with Controllable Thickness, (2002) 760–765.

[38] R. Kubrin, R.M. Pasquarelli, M. Waleczek, H.S. Lee, R. Zierold, J.J. Do Rosário, P.N. Dyachenko, J.M. Montero Moreno, A.Y. Petrov, R. Janssen, M. Eich, K. Nielsch, G.A. Schneider, Bottom-up Fabrication of Multilayer Stacks of 3D Photonic Crystals from Titanium Dioxide, ACS Appl. Mater. Interfaces. 8 (2016) 10466–10476. doi:10.1021/acsami.6b00827.

[39] Y. Habibi, A.L. Goffin, N. Schiltz, E. Duquesne, P. Dubois, A. Dufresne, Bionanocomposites based on poly(ε-caprolactone)-grafted cellulose nanocrystals by ring-opening polymerization, J. Mater. Chem. 18 (2008) 5002–5010. doi:10.1039/b809212e.

[40] K.E. Shopsowitz, J.A. Kelly, W.Y. Hamad, M.J. MacLachlan, Biopolymer templated glass with a twist: Controlling the chirality, porosity, and photonic properties of silica with cellulose nanocrystals, Adv. Funct. Mater. 24 (2014) 327–338. doi:10.1002/adfm.201301737.

[41] K.E. Shopsowitz, H. Qi, W. Information, Y. Hamad, M.J. MacLachlan, W.Y. Hamad, M.J. MacLachlan, Free-Standing Mesoporous Silica Films With Tunable Chiral Nematic Structures, Nature. 468 (2010) 1–7. doi:10.1038/nature09540.

[42] K.E. Shopsowitz, A. Stahl, W.Y. Hamad, M.J. MacLachlan, Hard templating of nanocrystalline titanium dioxide with chiral nematic ordering, Angew. Chemie - Int. Ed. 51 (2012) 6886–6890. doi:10.1002/anie.201201113.

[43] E. Paineau, M.S. Amara, G. Monet, V. Peyre, S. Rouzière, P. Launois, Effect of ionic strength on the bundling of metal oxide imogolite nanotubes, J. Phys. Chem. C. 121 (2017) 21740–21749. doi:10.1021/acs.jpcc.7b07391.

[44] C. Colbeau-Justin, M. Kunst, D. Huguenin, Structural influence on charge-carrier lifetimes in TiO2 powders studied by microwave absorption, J. Mater. Sci. 38 (2003) 2429–2437. doi:10.1023/A:1023905102094.

[45] S. Beck, M. Méthot, J. Bouchard, General procedure for determining cellulose nanocrystal sulfate half-ester content by conductometric titration, Cellulose. 22 (2015) 101–116. doi:10.1007/s10570-014-0513-y.

[46] E. Ureña-Benavides, C. Kitchens, Wide-Angle X-ray Diffraction of Cellulose Nanocrystal− Alginate Nanocomposite Fibers, Macromolecules. (2011) 3478–3484. http://pubs.acs.org/doi/abs/10.1021/ma102731m.

[47] J.F. Revol, H. Bradford, J. Giasson, R.H. Marchessault, D.G. Gray, Helicoidal self ordering of cellulose microfibrils in aqueous suspension, Int. J. Biol. Macromol. 14 (1992) 170. doi:1-s2.0-S014181300580008X.

[48] P.X. Wang, W.Y. Hamad, M.J. MacLachlan, Structure and transformation of tactoids in

cellulose nanocrystal suspensions, Nat. Commun. 7 (2016) 1–8. doi:10.1038/ncomms11515.

[49] P. Saha, V.A. Davis, Photonic Properties and Applications of Cellulose Nanocrystal Films with Planar Anchoring, ACS Appl. Nano Mater. 1 (2018) 2175–2183. doi:10.1021/acsanm.8b00233.

[50] S. Beck, J. Bouchard, G. Chauve, R. Berry, Controlled production of patterns in iridescent solid films of cellulose nanocrystals, Cellulose. 20 (2013) 1401–1411. doi:10.1007/s10570-013-9888-4.

[51] S.T. Martin, H. Herrmann, W. Choi, M.R. Hoffmann, Time-resolved Microwave Conductivity, J. Chem. Soc. 90 (1994) 3315–3322. doi:10.1039/ft9949003315.

[52] J.C. Brauer, A. Marchioro, A.A. Paraecattil, A.A. Oskouei, J.E. Moser, Dynamics of Interfacial Charge Transfer States and Carriers Separation in Dye-Sensitized Solar Cells: A Time-Resolved Terahertz Spectroscopy Study, J. Phys. Chem. C. 119 (2015) 26266–26274. doi:10.1021/acs.jpcc.5b06911.

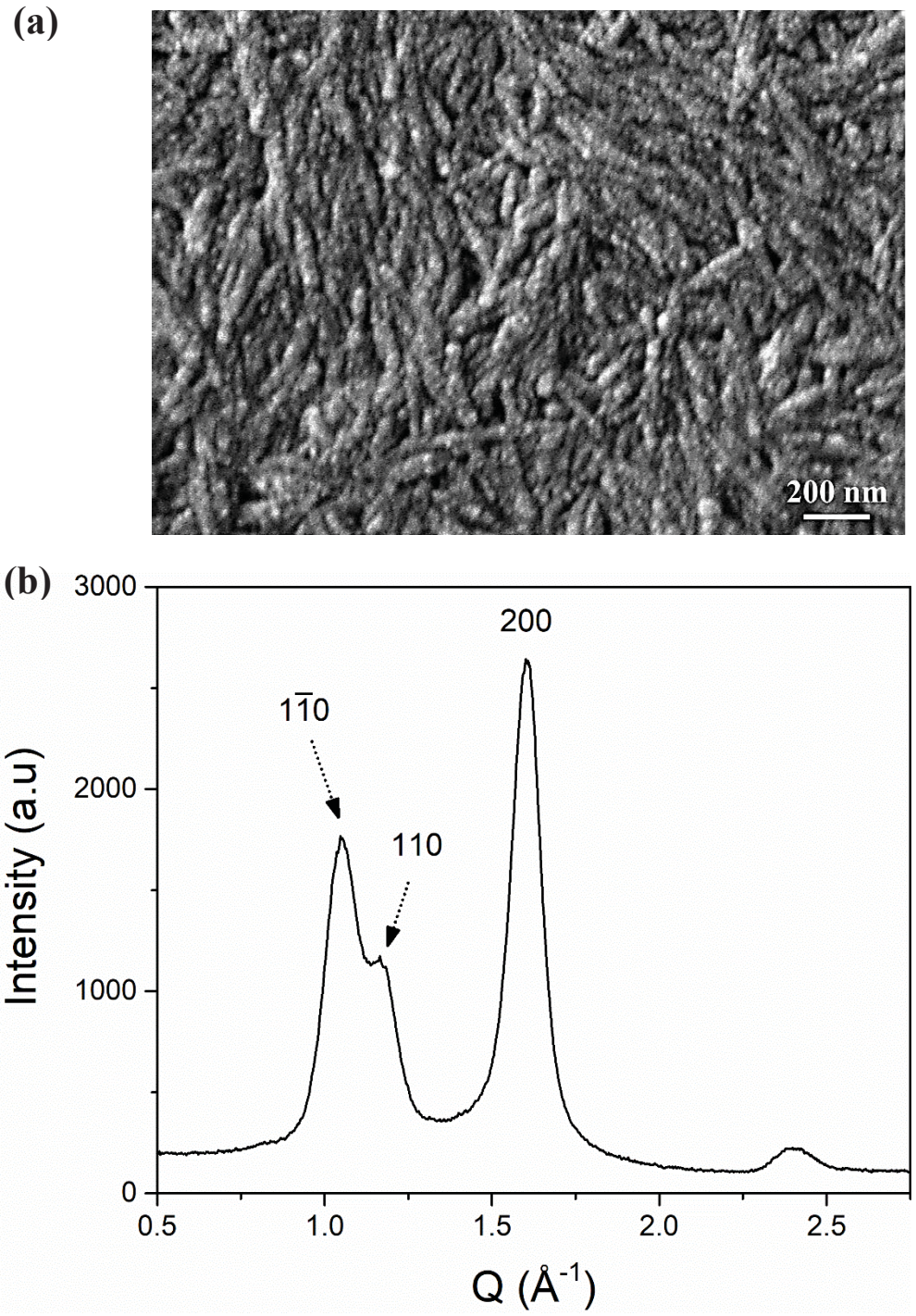

Figure 1. (a) SEM micrograph and (b) WAXS diagram obtained on a CNC film realized by the EISA method.

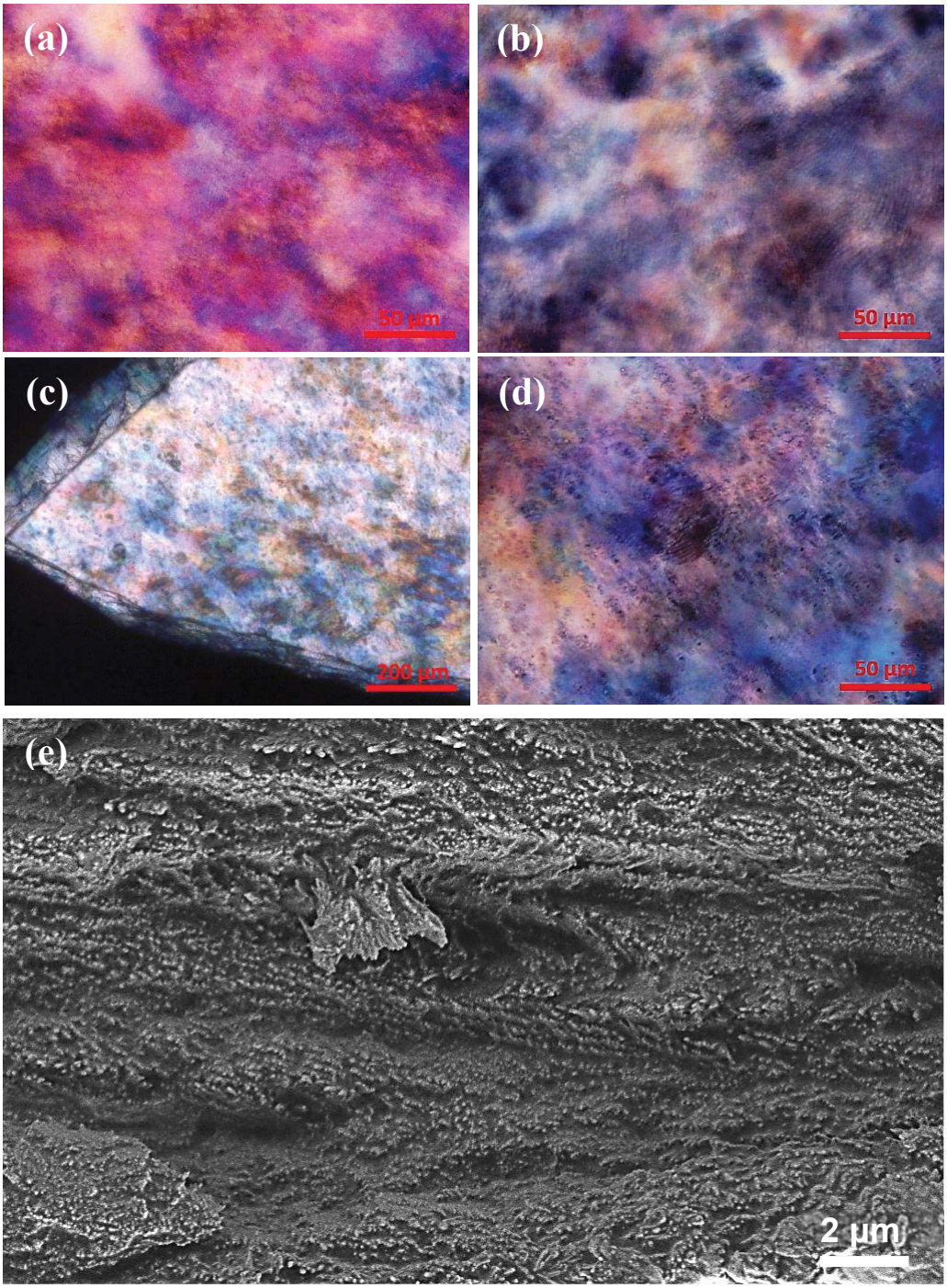

Figure 2. POM image of composite photonic films of SiO_2/CNCs in weight ratio 0.5(a), 1 (b) 2 (c) and 3 (d) showing the birefringence and the fingerprint of the chiral nematic structure. (e) SEM image of the cross section of composite SiO_2/CNCs films with a weight ratio of 2 showing the chiral nematic structure.

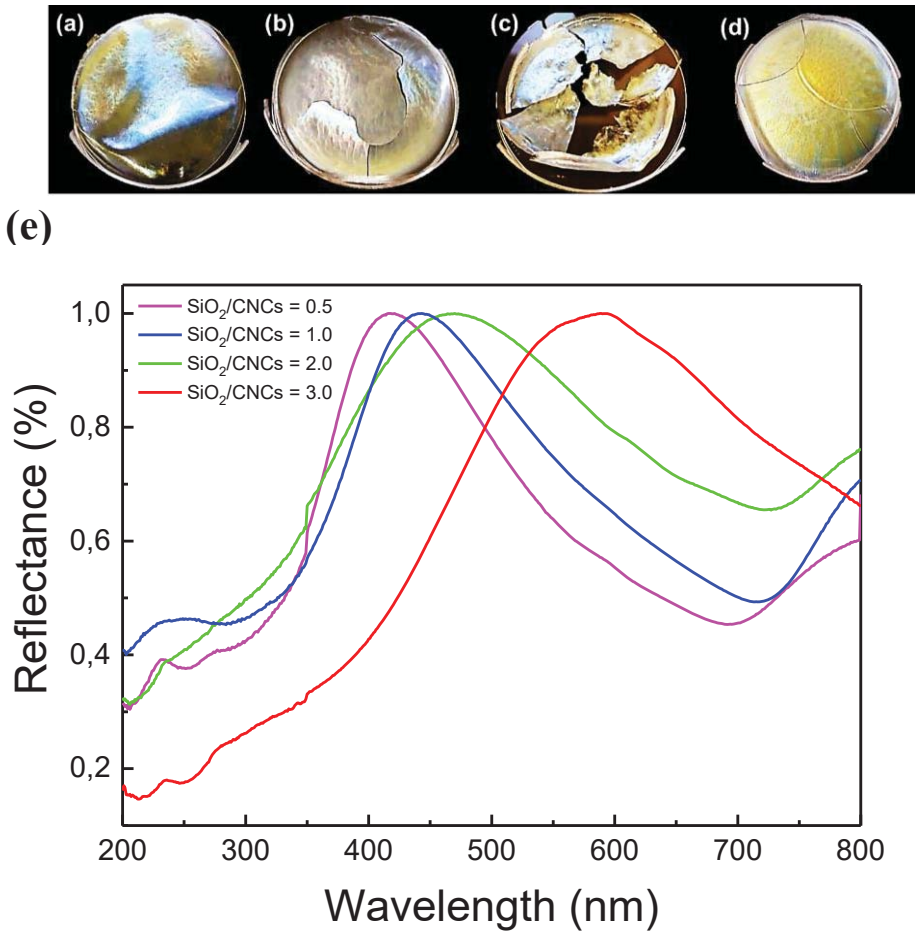

Figure 3: Photographs of SiO_2/CNCs composite films at weight ratio (a) 0.5 (b) 1 (c) 2 (d) 3 and (c) UV-vis reflectance spectra showing variable Bragg peak position red-shifted as the ratio of SiO_2/CNCs increases.

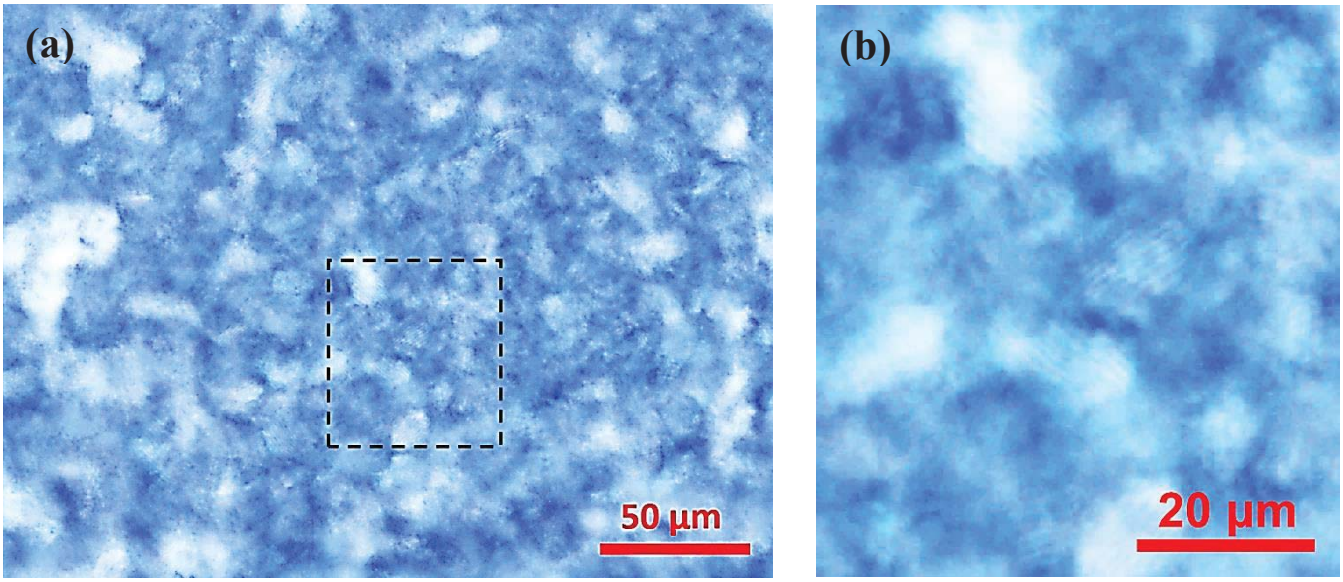

Figure 4: (a) POM observations of structure in the inorganic SiO_2 films showing birefringence(b) higher magnification of region in (a) evidences the fingerprint texture caracteristic of the chiral nematic ordering.

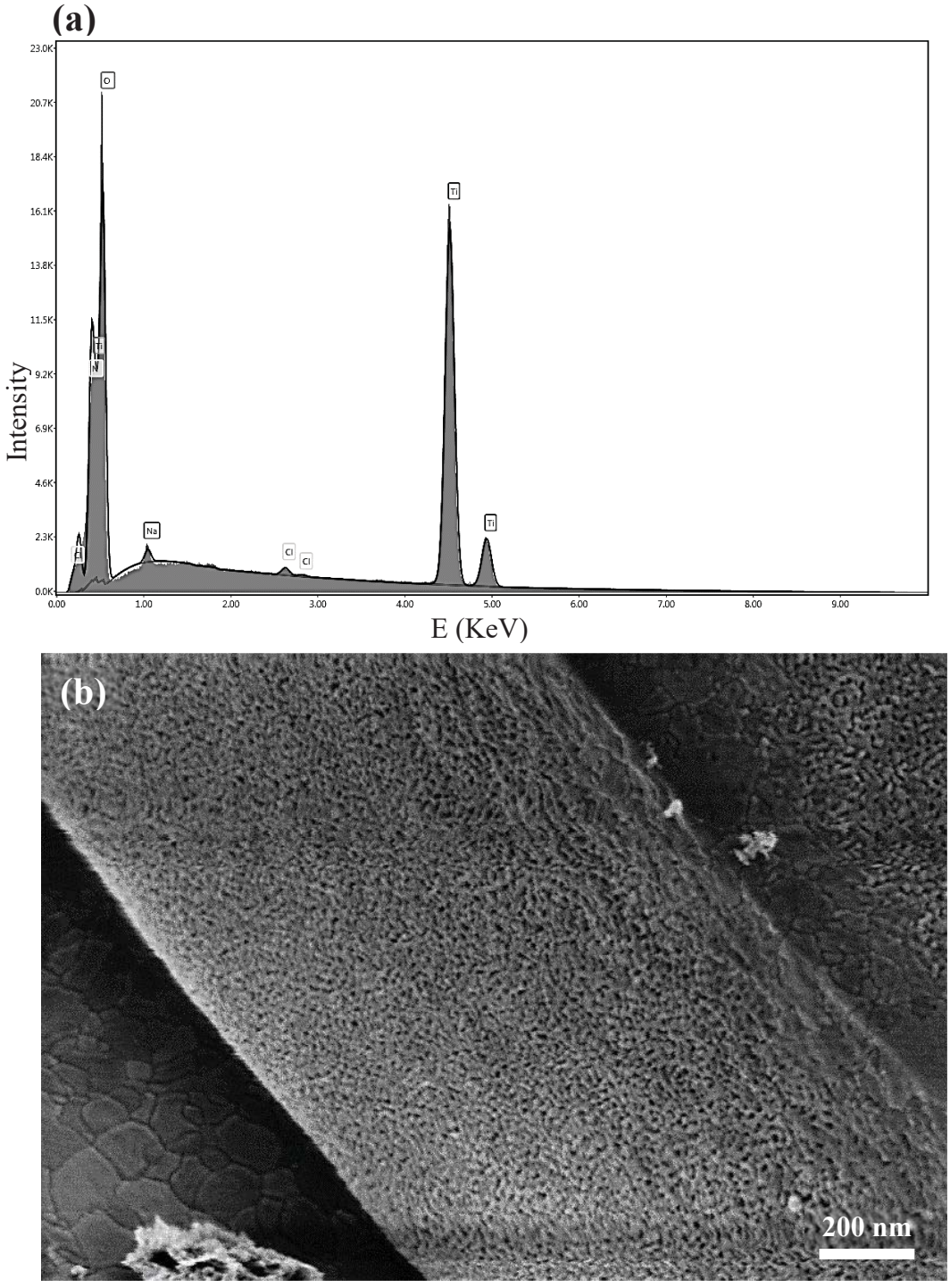

Figure 5: (a) EDX analysis of HT-TiO_2-2 film after the silica etching under basic solution. (b) SEM images of of the cross-section of HT-TiO_2 film.

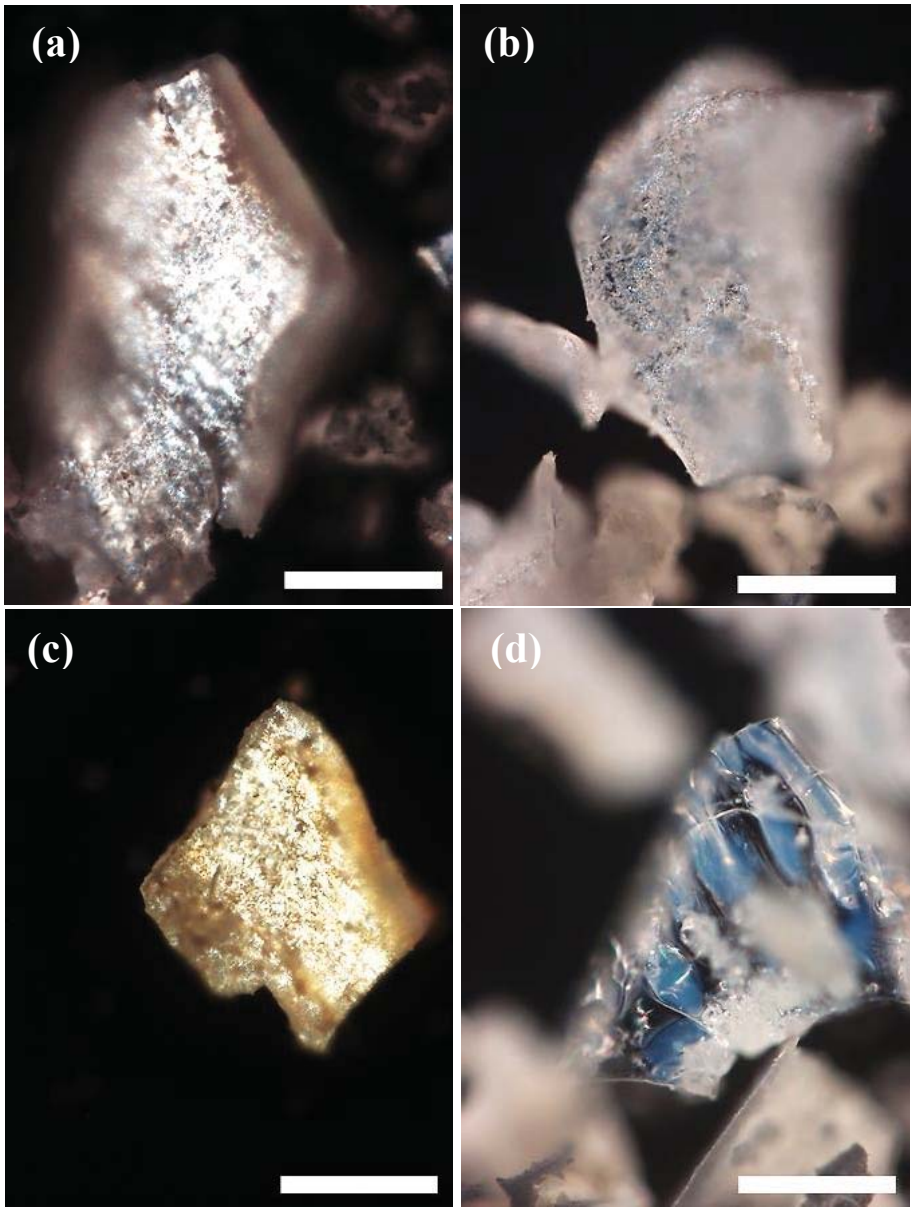

Figure 6: POM image of HT-TiO_2 films by two-step hard templating with variable ratio of SiO_2/CNCs: (a) 0.5 wt%, (b) 1 wt%, (c) 2 wt% (d) 3 wt%. Scale bar is 1 mm.

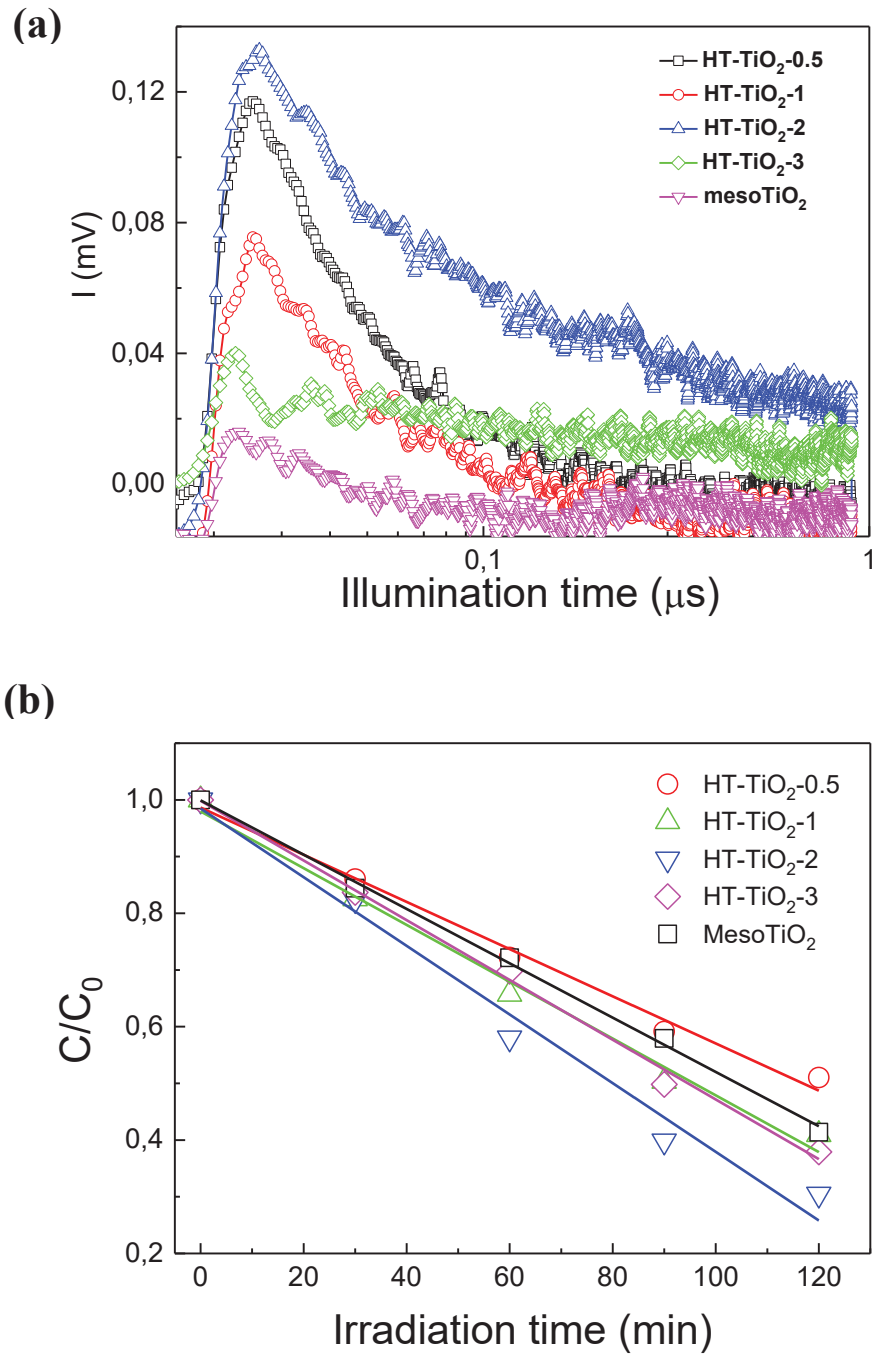

Figure 7: (a) TRMC signals of mesoporous TiO_2 and HT-TiO_2 after excitation at λ=360 nm. (b) Photocatalytic degradation of phenol (50 ppm) under UV-visible light for TiO_2 prepared via hard-templating and one-pot method.